



# CHORUS

This is the accepted manuscript made available via CHORUS. The article has been published as:

## Engineering the Spectrum of Dipole Field-Localized Spin-Wave Modes to Enable Spin-Torque Antidamping

Chi Zhang, Yong Pu, Sergei A. Manuilov, Shane P. White, Michael R. Page, Erick C. Blomberg, Denis V. Pelekhov, and P. Chris Hammel

Phys. Rev. Applied **7**, 054019 — Published 25 May 2017

DOI: [10.1103/PhysRevApplied.7.054019](https://doi.org/10.1103/PhysRevApplied.7.054019)

# Engineering the spectrum of dipole field-localized spin wave modes to enable spin-torque anti-damping

Chi Zhang, Yong Pu, Sergei A. Manuilov, Shane P. White, Michael R. Page, Erick C. Blomberg, Denis V. Pelekhov, and P. Chris Hammel\*  
*Department of Physics, The Ohio State University, Columbus, OH 43210, USA*  
(Dated: April 19, 2017)

Auto-oscillation of a ferromagnet due to spin-orbit torques in response to a dc current is of wide interest as a flexible mechanism for generating controllable high frequency magnetic dynamics. However, spin wave mode degeneracies and nonlinear magnon-magnon scattering impede coherent precession. Discretization of the spin wave modes can reduce this scattering. Spatial localization of the spin wave modes by the strongly inhomogeneous dipole magnetic field of a nearby spherical micromagnet provides variable spatial confinement, thus offering the option of systematic tunability of magnon spectrum for studying multi-mode interactions. Here we demonstrate that field localization generates a discrete spin wave mode spectrum observable as a series of well-resolved localized modes in the presence of imposed spin currents arising from the spin Hall effect (SHE) in a permalloy/platinum (Py/Pt) microstrip. The observation of linewidth reduction through damping control in this micromagnetically engineered spectrum demonstrates that localized modes can be controlled efficiently, an important step toward continuously tunable SHE driven auto-oscillators.

## I. INTRODUCTION

Spin-torques generated by spin currents imposed on a ferromagnet (FM) can reduce damping to the point of inducing auto-oscillation, enabling a frequency-tunable microwave source, a scientifically and technologically powerful tool [1]. Spin currents generated by spin-orbit effects such as the spin Hall effect [2–4] offer a simple planar geometry that is easily fabricated and avoids scaling issues that encumber magnetic tunnel junction (MTJ) based structures [5]. Spin-Hall driven auto-oscillation of the quasi-uniform mode in an extended ferromagnetic film with uniformly applied spin-torque has been hampered by nonlinear magnon scattering processes that redistribute energy from the desired mode into a large number of degenerate spin wave modes [6]. Spin-Hall oscillators demonstrated to date have utilized either local, nanoscale excitation of a mode whose resonance frequency lies below the continuous spin wave dispersion of the extended FM film [2, 7–9], or have geometrically confined the excited mode (in, e.g., a nanowire) so that the degeneracies of the spin wave dispersion are strongly lifted [3, 10, 11]. The ability to engineer the magnon spectrum could permit systematic tuning of multi-mode interactions and detailed study of their implications for spin-Hall oscillators.

Here we describe the use of tunable, magnetic field-localized modes to define the magnon spectrum of a ferromagnetic element, enabling spin-Hall torque induced damping control. Localized spin wave modes, confined by the strongly inhomogeneous dipole magnetic field of a nearby scanned micromagnet, have been demonstrated in ferromagnetic resonance force microscopy (FMRFM) for both imaging and studies of magnetization dynamics at

the nanoscale [12–14]. Using magnetic field-localization to define the eigen-modes of a spin-Hall oscillator offers a new approach to the study of spin-Hall torque physics, and multi-mode interactions. As a set of discrete spin wave modes with frequencies below the quasi-uniform mode, the localized excitations present a reduced number of magnon scattering channels [10]. Furthermore, the frequency separation of the localized mode resonances from their neighbors and the quasi-uniform mode can be systematically tuned by particle size and particle-sample separation; in particular, confinement parameters can be continuously tuned by scanning the separation between a scanned tip and the sample. Finally, field localized modes avoid the potential spurious effects arising from fabrication edge damage [15, 16] associated with lithographically defined structures.

Here we report electrical spin-torque ferromagnetic resonance (ST-FMR) measurements of well-resolved localized modes in a Py/Pt microstrip. We show that magnon spectral engineering by means of a micromagnetic particle enables damping control by an imposed DC current. This approach allows thorough characterization of the relevant (nearby in frequency) magnon modes in addition to the quasi-uniform mode; in particular, we find that the linewidth of the localized modes can be controlled efficiently by the spin-Hall torque.

## II. METHODS

Py (5 nm)/Pt (5 nm) films are deposited on an undoped Si substrate by e-beam evaporation. The resistivities of the Py and Pt are estimated to be  $50 \mu\Omega \cdot \text{cm}$  and  $40 \mu\Omega \cdot \text{cm}$ , respectively, from studies of various Py and Py/Pt stacks. The bilayer films are patterned into microstrips ( $3 \mu\text{m} \times 3 \mu\text{m}$  and  $3 \mu\text{m} \times 6 \mu\text{m}$ ) via photolithography and ion milling. A broadband microwave coplanar stripline (CPS) is fabricated on the same Si sub-

---

\* hammel@physics.osu.edu

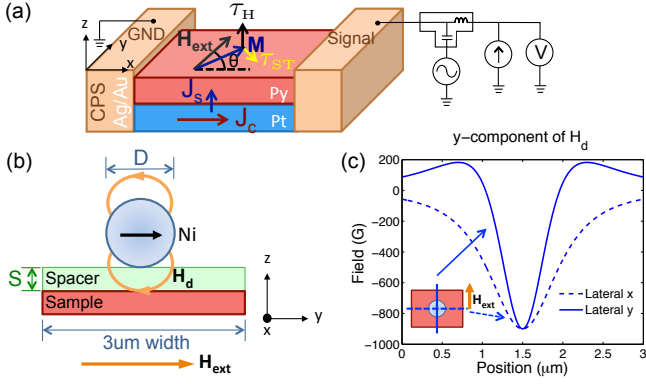


FIG. 1. (a) Schematic of ST-FMR setup, illustrating orientations of the damping torque  $\tau_\alpha$ , spin-torque  $\tau_{ST}$  and torque from the Oersted field  $\tau_H$ . Here, the external field  $H_{ext}$  and  $M$  lie in the plane and  $\theta$  denotes the in-plane angle between  $H_{ext}$  and the direction of the applied current in the microstrip. (b) Side view of a micromagnetic particle of a diameter  $D$ , glued onto a spacer of thickness  $S$  separating it from the sample, depicted for  $H_{ext}$  at  $\theta = 90^\circ$ . (c) Corresponding to the configuration in (b), the plotted curves are spatial profiles of the  $y$ -component of dipole field,  $H_d$ , from a  $1 \mu\text{m}$  Ni particle (with saturated moment,  $0.15 \mu\text{m}$  particle-sample separation) as a function of lateral  $x$  or  $y$  position in the Py/Pt sample plane under the particle. Dimensions used in (b) and (c) are associated with experiments shown in Fig. 3.

strate using photolithographic lift-off so that each Py/Pt microstrip is part of the CPS, as an electrical load connecting the signal line to the ground line of CPS. The modes are localized by the dipole field of a micromagnetic particle located at two distances above the sample determined by deposited spacers: we spin either a layer of photoresist S1805 as a  $0.45 \mu\text{m}$  spacer or PMMA as a  $0.15 \mu\text{m}$  spacer, and subsequently glue a  $5 \mu\text{m}$  or  $1 \mu\text{m}$  diameter nickel (Ni) spherical particle above the center of the microstrip [Fig. 1(b)]. All of our measurements are performed at room temperature. As depicted in Fig. 1(a), a charge current density  $J_C$  applied along the strip in the Pt layer is converted into a transverse spin current density  $J_S$  due to the spin-Hall effect (SHE) [17, 18]. The spin current is injected into the Py layer and exerts a spin torque (ST) [19, 20] on the Py magnetization. We simultaneously apply a modulated microwave charge current  $I_{RF}$  at a fixed frequency  $f$  while sweeping the external field.  $I_{RF}$  generates an ac-Oersted field torque  $\tau_H$  as well as an ac-spin-Hall torque  $\tau_{ST}$  [21] which drives various eigenmodes into precession in the Py strip. A particular mode, either localized or quasi-uniform (hereafter “quasi-uniform” will refer to the mode in the Py strip, but away from the micromagnet), is excited when the frequency of  $I_{RF}$  matches the magnetic resonance condition defined by the applied magnetic field. Precession results in an ac-variation of the resistance  $\delta R_{ac}$  due to anisotropic magnetoresistance (AMR). Mixing between  $I_{RF}$  and  $\delta R_{ac}$  [21–23] produces a dc voltage  $V_{mix}$ , which is detected via a

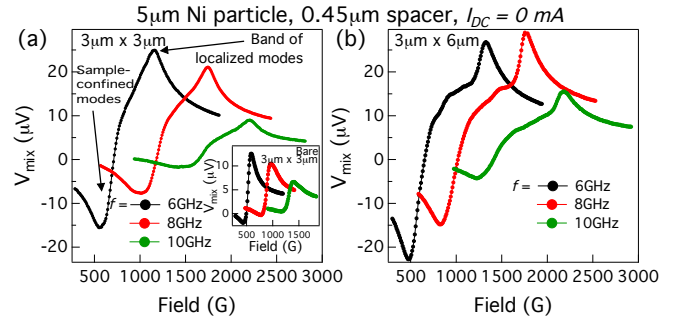


FIG. 2. ST-FMR spectra taken with the  $5 \mu\text{m}$  Ni particle on a  $3 \mu\text{m}$ -wide strip, with a  $0.45 \mu\text{m}$  photoresist S1805 spacer, at  $I_{DC} = 0 \text{ mA}$ ,  $H_{ext}$  applied at  $45^\circ$ , and frequencies from 6 to 10 GHz, at an RF power of 6 dBm. (a)  $3 \mu\text{m} \times 3 \mu\text{m}$  strip. Inset: ST-FMR spectra of a bare  $3 \mu\text{m} \times 3 \mu\text{m}$  strip at 6 to 10 GHz, at an RF power of 0 dB. (b)  $3 \mu\text{m} \times 6 \mu\text{m}$  strip.

lock-in amplifier.  $V_{mix}$  can be fitted with symmetric and anti-symmetric Lorentzian functions, arising from the ac-spin current and ac-Oersted field, respectively [21]. In addition to  $I_{RF}$ , we also apply a DC charge current  $I_{DC}$  that generates a dc-spin torque. This torque can either enhance or suppress the damping of the mode thus modifying its linewidth in the FMR spectrum [21, 22]. The external field  $H_{ext}$  is applied in the film plane, at an angle  $\theta$  with respect to direction of current flow along the length of the strip. For  $I_{DC} = 0$ , the angle  $\theta$  is set to  $45^\circ$  where the Py AMR signal is maximized. When  $I_{DC}$  is applied, the effect of SHE-induced ST is maximized at  $90^\circ$ , so measurements are performed at  $\theta = 70^\circ$  to balance AMR and ST [7, 9]. The low-coercivity [24] Ni particle is magnetized parallel to  $H_{ext}$ , so the sample experiences a dipole field  $H_d$  anti-parallel to  $H_{ext}$ , creating a spatial field-well. Figs. 1(b) and (c) show the field orientations and the cross-section plots of the  $y$ -component of the dipole field  $H_d$  ( $\theta = 90^\circ$ , *i.e.*,  $H_{ext}$  in the  $y$ -direction), as a function of lateral  $x$  or  $y$  position in the sample plane. The field-well is more confined in the  $H_{ext}$ -direction, resulting in elongated localized modes underneath the particle.

### III. RESULTS

In this section, we show results for localized modes confined by Ni particles having different sizes and particle-sample separations. We focus on the  $1 \mu\text{m}$  particle, and discuss the  $5 \mu\text{m}$  Ni particle only briefly.

Comparison of ST-FMR spectra in the case of the larger,  $5 \mu\text{m}$ , Ni particle on the  $3 \mu\text{m} \times 3 \mu\text{m}$  strip and  $3 \mu\text{m} \times 6 \mu\text{m}$  strip, shown in Fig 2(a) and (b) with those from the bare  $3 \mu\text{m}$ -width strip (in the figure inset) reveals an additional peak on the higher field side as expected for localized modes [12–14]. We performed micromagnetic modeling [12, 25–27] to determine that the highest field modes are a set of localized modes [Fig.

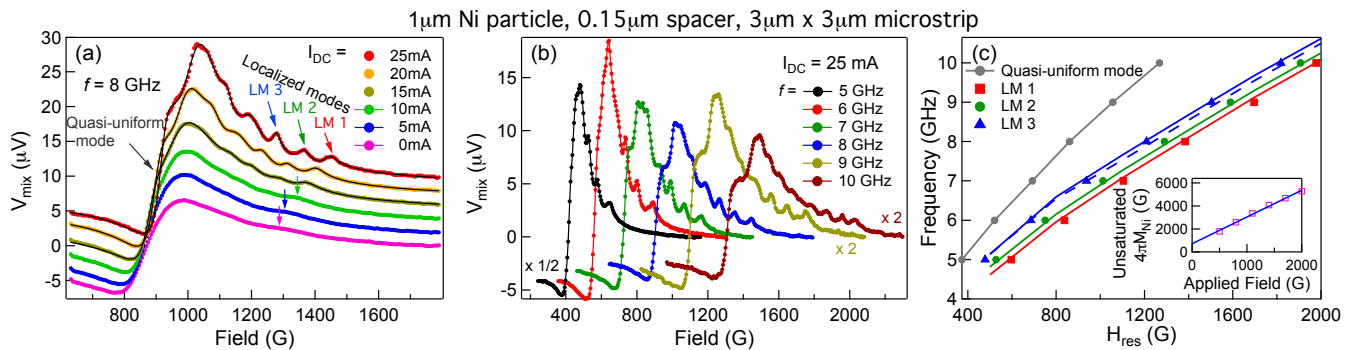


FIG. 3. Evolution of the ST-FMR spectra with  $I_{DC}$  and frequency, taken with a  $1 \mu\text{m}$  Ni particle separated from the  $3 \mu\text{m} \times 3 \mu\text{m}$  strip by a  $0.15 \mu\text{m}$  PMMA spacer, and  $H_{\text{ext}}$  applied at  $70^\circ$ . (a)  $f = 8\text{GHz}$ , for  $I_{DC}$  increasing from 0 to 25 mA, all at an RF power of 0 dBm. The three lowest-energy localized modes (LM) are labeled as LM1, LM2 and LM3. The black curves for spectra above 15 mA are representative multi-peak Lorentzian fits. (b) Spectra of well-resolved localized modes at  $I_{DC} = 25 \text{ mA}$ , at RF powers of -3 dBm (5, 9 and 10 GHz spectra were rescaled to maximize figure details). (c) Frequency versus field plots for the resonant quasi-uniform mode and the first three localized modes. The symbols ( $\circ$   $\square$   $\triangle$ ) show experimental  $H_{\text{res}}$  data extracted from Fig. 3(b), reduced by 50 G to account for the Oersted field and heating from  $I_{DC}$  (determined by the shift of the quasi-uniform mode). The curves for the localized modes show the results of micromagnetic simulations, ignoring spin-torque effects (*i.e.* for  $I_{DC} = 0$ ):  $n = 1$  (red),  $n = 2$  (green),  $n = 1, m = 2$  (dotted blue), and  $n = 3$  (solid blue). Inset: Effective magnetization of the unsaturated Ni particle used at each external field to give the simulation results in Fig. 3(c), which agrees with the known hysteresis loop of a Ni particle [24]. The solid line is a linear fit, yielding  $4\pi M_{\text{Ni}} = 2.3H + 722.9$  Gauss.

4(c)]. The broad peak observed from localized modes [12–14, 28] indicates that they are a band of localized modes, closely spaced and thus have overlapping spectra [for details of the spectral separation of the localized modes see the Discussion A section]. For a particle diameter larger than the microstrip dimension, the lower-field peak corresponds to spin wave modes that are confined by the sample, but whose mode amplitudes are globally modified by the particle-field, which we will not further discuss here.

In order to observe individual localized modes, we placed a smaller  $1 \mu\text{m}$  Ni particle closer to the sample,  $0.15 \mu\text{m}$ , to increase the spectral separation of the various localized mode resonances [see Discussion A]. Additionally, we can narrow the linewidth of the localized modes to further improve their resolvability with an anti-damping spin-Hall torque. With the frequency of  $I_{\text{RF}}$  fixed at 8 GHz, the bottom pink curve in Fig. 3(a) shows the resulting spectrum obtained for  $I_{DC} = 0 \text{ mA}$ . We observe a resonance from the quasi-uniform mode, and a shoulder at higher field, indicating localized modes. Applying a DC current  $I_{DC}$  allows study of the damping control by the spin-Hall torque. A positive sign of  $I_{DC}$  corresponds to an anti-damping torque. The localized modes are not individually resolvable below 15 mA (including negative currents), because the linewidth of the modes exceeds or is just comparable to their separation. At 15 mA ( $J_{DC} \approx 5.6 \times 10^{11} \text{ Am}^{-2}$ ), we observe several weakly-resolved localized modes. At 25 mA ( $J_{DC} \approx 9.3 \times 10^{11} \text{ Am}^{-2}$ ), the localized modes become well-resolved. At fixed  $I_{DC} = 25 \text{ mA}$  we take spectra at several frequencies; all display well-resolved localized modes [Fig. 3(b)]. We extract the resonance field  $H_{\text{res}}$  by multi-

peak Lorentzian fits and plot them in Fig. 3(c). To identify the localized modes resonances, we performed micromagnetic modeling [12, 25–27] at  $\theta = 70^\circ$ , using a value of  $4\pi M_{\text{eff}} = 8.7 \text{ kG}$ , determined from the in-situ Py/Pt film (both at  $I_{DC} = 0$ ). For a Py thickness of 5 nm, the four lowest-energy localized modes are three width modes ( $n = 1, 2, 3$ ) [13] and one higher-order length mode ( $n = 1, m = 2$ ). Here,  $n$  and  $m$  label the mode number for the mode width and length directions respectively [see Fig. 4(d)]. The first higher-order length mode is comparable in energy to the  $n = 3$  width mode and is therefore included in the analysis. The solid curves for localized modes in the Fig. 3(c) show simulation results for these four candidates for the first three localized mode peaks in the experimental spectrum. We note that the moment of the Ni particle is not saturated at external fields below 2000 G. The Ni magnetization was varied [13] as a free parameter in the simulation [Fig.3 (c) inset].

## IV. DISCUSSION

### A. Localized modes separation vs. particle size and particle-sample separation

The spectral separation between localized modes is controlled by the confinement by the internal static field-well, illustrated in Fig. 4(a) and (b). The spatial profile of the internal static field is dominated by 1) the uniform external field, 2) the dipole field from the micromagnetic particle and 3) the demagnetizing field mainly at sample edges. A smaller micromagnetic particle brought closer to the sample will lead to a spatially narrower

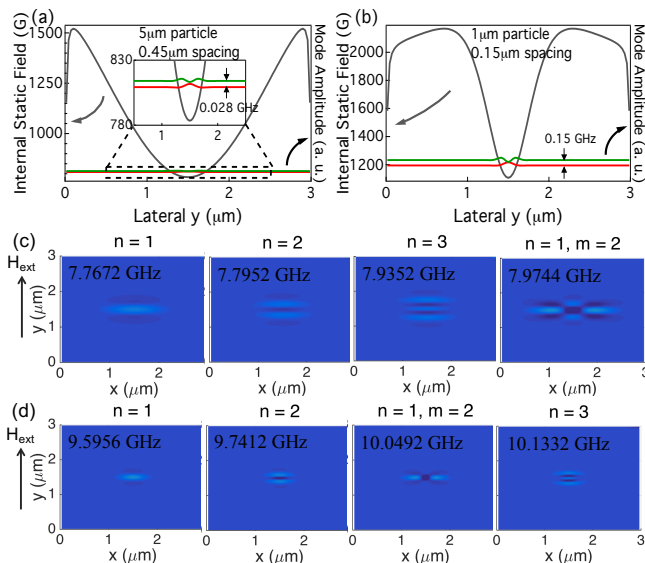


FIG. 4. (a), (b) Spatial variation of the internal static field (grey) and mode amplitudes of the  $n = 1$  (red) and  $n = 2$  (green) localized mode profiles plotted versus lateral position in the  $H_{\text{ext}}$ -direction. (c), (d) Spatial profiles of transverse magnetization of the localized modes for a  $5 \mu\text{m}$  particle,  $0.45 \mu\text{m}$  particle-sample separation (c) and a  $1 \mu\text{m}$  particle,  $0.15 \mu\text{m}$  particle-sample separation (d). The micromagnetic simulations assume the Ni particles are saturated. (see inset to Fig 3c),  $H_{\text{ext}} = 2000 \text{ G}$  at  $\theta = 90^\circ$ . The mode elongation in the direction perpendicular to the applied field (see text) is evident.

dipole field-well. The dynamic modes confined by internal static fields are analogous to quantum mechanical wave functions in a potential-well [25, 29], in particular the narrower the field-well, the larger the energy separation between the localized modes. The micromagnetic simulations at  $H_{\text{ext}} = 2000 \text{ G}$  find that the average separation between the first three localized width modes ( $n = 1, 2, 3$ ) at fixed external field is  $0.084 \text{ GHz}$  (roughly  $24 \text{ G}$  converted into field separation) for the  $5 \mu\text{m}$  particle ( $0.45 \mu\text{m}$  particle-sample separation), and  $0.27 \text{ GHz}$  (roughly  $77 \text{ G}$  converted into field separation) for the  $1 \mu\text{m}$  particle ( $0.15 \mu\text{m}$  particle-sample separation). Mode profiles are shown in Fig. 4(c) and (d), corresponding to the experiments in Fig. 2 and Fig. 3, respectively.

### B. Spin-Hall torque on localized modes

Next we discuss the influence of spin-Hall torque on different modes. The DC current has two consequences. Firstly, positive  $I_{\text{DC}}$  significantly narrows the linewidth of all the modes. In Fig. 5(a), the linewidths  $\Delta H$  of the quasi-uniform and first three localized modes at  $8 \text{ GHz}$  are plotted as a function of  $I_{\text{DC}}$ . The slope of the linewidth variation with  $I_{\text{DC}}$  is similar for all modes. An estimate of the critical current density for the first three localized modes (where linewidth extrapolates to zero)

is  $J_{\text{cri}} \approx 1.4 \times 10^{12} \text{ Am}^{-2}$  at  $8 \text{ GHz}$ , which is typical for metallic systems [2, 21], and indicates that damping of the localized modes can be controlled efficiently by the spin-Hall current.

Secondly,  $I_{\text{DC}}$  shifts the resonances to higher fields. We plot the resonance field  $H_{\text{res}}$  as a function of  $I_{\text{DC}}$  in Fig. 5(b). At low currents, the mode shift arises from the dc-Oersted field generated by the dc-current in the Pt layer [5, 6, 30]. For microstrips, the current density is essentially homogeneous, and thus the Oersted field will be constant across the sample, shifting all modes by the same amount. This shift will be linear in  $I_{\text{DC}}$ , and is calculated to be  $\sim 1.2 \text{ G/}\mu\text{A}$  [5, 30]. At high currents, Joule heating and more interesting nonlinear ST effects [5, 6, 30, 31] further enhance the shifts. To compare the latter  $H_{\text{res}}$  shifts between different modes, we plot the change in  $H_{\text{res}}$  relative to the  $H_{\text{res}}$  value at  $15 \text{ mA}$  for each mode in the Fig. 5(c), all corrected by the contribution of the Oersted field. We observe a significant difference in the evolution of the localized modes relative to the quasi-uniform mode. Joule heating increases the device temperature [32], thus reducing the effective magnetization of Py, and hence shifting the quasi-uniform mode. From the shift  $H_{\text{res}}$  of the quasi-uniform mode due to Joule heating we know the change in effective magnetization. Knowing this we can calculate the expected shift of the localized mode resonances, shown by the grey curve in the inset to Fig. 5(c). The shift of the localized modes due to Joule heating is slightly larger than for the quasi-uniform mode, but this cannot explain the experimentally observed shifts, which are two to three times larger than that of the quasi-uniform mode. This larger shift of the localized modes indicates that their opening cone angle is enhanced relative to the quasi-uniform mode for a given spin-Hall torque [31]. We note that, along with the significant linewidth reduction, this increased shift improves the resolvability of the localized modes as they are shifted away from the quasi-uniform mode.

## V. CONCLUSIONS

In summary, we have demonstrated the first electrical ST-FMR detection of well-resolved, magnetic field-defined localized modes. We engineered their mode separation by varying the size of the particle that produces the localizing field and the particle-sample separation. This tunability of the localized modes potentially provides a platform for understanding the multi-mode interaction mechanism in spin-Hall oscillators, and for optimizing spin-Hall oscillators as spintronics devices. Additionally, we achieved significant linewidth reduction of localized modes by means of anti-damping spin-Hall torque, and find that their linewidth can be controlled efficiently. This can aid study of spin dynamics of localized modes by improving spectral resolution. Finally, the eigenmodes of our device consist of a set of quasi-

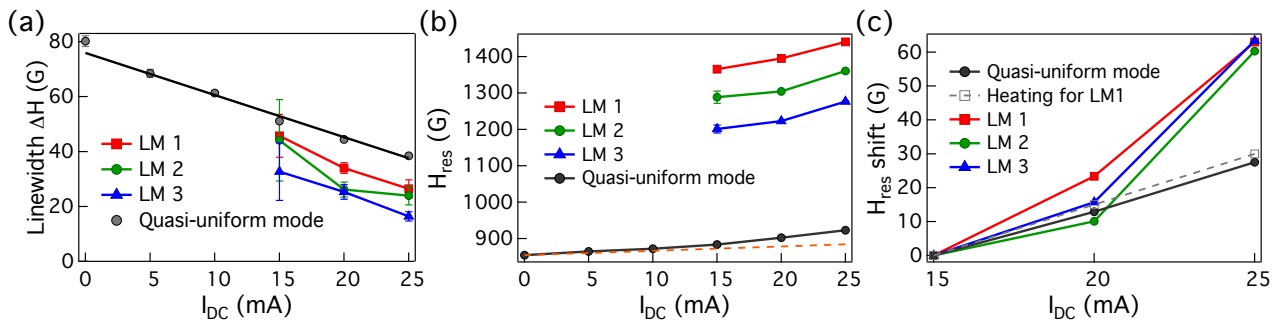


FIG. 5. (a), (b) Dependencies of the extracted linewidth  $\Delta H$  and resonance field  $H_{\text{res}}$  on  $I_{\text{DC}}$  from Fig. 3(a) for the quasi-uniform mode and first three localized modes. The line in (a) is a linear fit. The dc-Oersted field shift is shown by the dashed line in (b). (c)  $H_{\text{res}}$  shift relative to resonance value at 15 mA, corrected by the field shift contribution due to the dc-Oersted field. The grey curve shows the calculated  $H_{\text{res}}$  shift for LM1 due to Joule heating.

continuous spin wave modes in the microstrip in proximity to a set of discrete localized modes confined by the particle-field; this provides an opportunity to study the coupling of localized mode to the continuum of surrounding spin wave modes [12].

## ACKNOWLEDGMENTS

This work was primarily supported by the US Department of Energy (DOE), Office of Science, Basic Energy Sciences, under Award No. DE-FG02-03ER46054 (experiment design, device fabrication, data acquisition and analysis). This work was supported in part by the Center for Emergent Materials, an NSF-funded MRSEC under Award No. DMR-1420451 (sample fabrication, characterization, data analysis). This work was supported in part by an allocation of computing time from the Ohio Supercomputer Center. We also acknowledge technical support and assistance provided by the NanoSystems Laboratory at the Ohio State University.

- 
- [1] S. I. Kiselev, J. C. Sankey, I. N. Krivorotov, N. C. Emley, R. J. Schoelkopf, R. A. Buhrman, and D. C. Ralph, Microwave oscillations of a nanomagnet driven by a spin-polarized current, *Nature* **425**, 380–383 (2003).
  - [2] V. E. Demidov, S. Urazhdin, H. Ulrichs, V. Tiberkevich, A. Slavin, D. Baither, G. Schmitz, and S. O. Demokritov, Magnetic nano-oscillator driven by pure spin current, *Nat. Mater.* **11**, 1028–1031 (2012).
  - [3] L. Liu, C.-F. Pai, D. C. Ralph, and R. A. Buhrman, Magnetic Oscillations Driven by the Spin Hall Effect in 3-Terminal Magnetic Tunnel Junction Devices, *Phys. Rev. Lett.* **109**, 186602 (2012).
  - [4] M. Collet, X. de Milly, O. d’Allivy Kelly, V. V. Naletov, R. Bernard, P. Bortolotti, J. Ben Youssef, V. E. Demidov, S. O. Demokritov, J. L. Prieto, M. Munoz, V. Cros, A. Anane, G. de Loubens, and O. Klein, Generation of coherent spin-wave modes in yttrium iron garnet microdisks by spin-orbit torque, *Nat. Commun.* **7** (2016).
  - [5] Z. Duan, C. T. Boone, X. Cheng, I. N. Krivorotov, N. Reckers, S. Stienen, M. Farle, and J. Lindner, Spin-wave modes in permalloy/platinum wires and tuning of the mode damping by spin Hall current, *Phys. Rev. B* **90**, 024427 (2014).
  - [6] V. E. Demidov, S. Urazhdin, E. R. J. Edwards, M. D. Stiles, R. D. McMichael, and S. O. Demokritov, Control of Magnetic Fluctuations by Spin Current, *Phys. Rev. Lett.* **107**, 107204 (2011).
  - [7] V. E. Demidov, S. Urazhdin, A. Zholud, A. V. Sadovnikov, and S. O. Demokritov, Nanoconstriction-based spin-Hall nano-oscillator, *Appl. Phys. Lett.* **105**, 172410 (2014).
  - [8] V. E. Demidov, S. Urazhdin, A. Zholud, A. V. Sadovnikov, A. N. Slavin, and S. O. Demokritov, Spin-current nano-oscillator based on nonlocal spin injection, *Sci. Rep.* **5**, 8578 (2015).
  - [9] R. H. Liu, W. L. Lim, and S. Urazhdin, Spectral Characteristics of the Microwave Emission by the Spin Hall Nano-Oscillator, *Phys. Rev. Lett.* **110**, 147601 (2013).
  - [10] Z. Duan, A. Smith, L. Yang, B. Youngblood, J. Lindner, V. E. Demidov, S. O. Demokritov, and I. N. Krivorotov, Nanowire spin torque oscillator driven by spin orbit torques, *Nat. Commun.* **5**, 5616 (2014).
  - [11] L. Yang, R. Verba, V. Tiberkevich, T. Schneider, A. Smith, Z. Duan, B. Youngblood, K. Lenz, J. Lindner, A. N. Slavin, and I. N. Krivorotov, Reduction of phase noise in nanowire spin orbit torque oscillators, *Sci. Rep.* **5**, 16942 (2015).

- [12] R. Adur, C. Du, H. Wang, S. A. Manuilov, V. P. Bhalamudi, C. Zhang, D. V. Pelekhov, F. Yang, and P. C. Hammel, Damping of Confined Modes in a Ferromagnetic Thin Insulating Film: Angular Momentum Transfer across a Nanoscale Field-Defined Interface, *Phys. Rev. Lett.* **113**, 176601 (2014).
- [13] H.-J. Chia, F. Guo, L. M. Belova, and R. D. McMichael, Nanoscale Spin Wave Localization Using Ferromagnetic Resonance Force Microscopy, *Phys. Rev. Lett.* **108**, 087206 (2012).
- [14] I. Lee, Y. Obukhov, G. Xiang, A. Hauser, F. Yang, P. Banerjee, D. V. Pelekhov, and P. C. Hammel, Nanoscale scanning probe ferromagnetic resonance imaging using localized modes, *Nature* **466**, 845–848 (2010).
- [15] S. Noh, D. Monma, K. Miyake, M. Doi, T. Kaneko, H. Imamura, and M. Sahashi, Spin Dynamics in Ferromagnetic Resonance for Nano-Sized Magnetic Dot Arrays: Metrology and Insight Into Magnetization Dynamics, *IEEE Trans. Magn.* **47**, 2387–2390 (2011).
- [16] J. M. Shaw, T. J. Silva, M. L. Schneider, and R. D. McMichael, Spin dynamics and mode structure in nanomagnet arrays: Effects of size and thickness on linewidth and damping, *Phys. Rev. B* **79**, 184404 (2009).
- [17] M. I. D’Yakonov and V. I. Perel’, Possibility of Orienting Electron Spins with Current, *JETP Lett.* **13**, 467 (1971).
- [18] J. E. Hirsch, Spin Hall Effect, *Phys. Rev. Lett.* **83**, 1834–1837 (1999).
- [19] L. Berger, Emission of spin waves by a magnetic multilayer traversed by a current, *Phys. Rev. B* **54**, 9353–9358 (1996).
- [20] J. C. Slonczewski, Current-driven excitation of magnetic multilayers, *J. Magn. Magn. Mater.* **159**, L1–L7 (1996).
- [21] L. Liu, T. Moriyama, D. C. Ralph, and R. A. Buhrman, Spin-Torque Ferromagnetic Resonance Induced by the Spin Hall Effect, *Phys. Rev. Lett.* **106**, 036601 (2011).
- [22] J. C. Sankey, P. M. Braganca, A. G. F. Garcia, I. N. Krivorotov, R. A. Buhrman, and D. C. Ralph, Spin-Transfer-Driven Ferromagnetic Resonance of Individual Nanomagnets, *Phys. Rev. Lett.* **96**, 227601 (2006).
- [23] A. A. Tulapurkar, Y. Suzuki, A. Fukushima, H. Kubota, H. Maehara, K. Tsunekawa, D. D. Djayaprawira, N. Watanabe, and S. Yuasa, Spin-torque diode effect in magnetic tunnel junctions, *Nature* **438**, 339–342 (2005).
- [24] H.-J. Song, X.-H. Jia, X.-F. Yang, H. Tang, Y. Li, and Y.-T. Su, Controllable synthesis of monodisperse polyhedral nickel nanocrystals, *CrystEngComm* **14**, 405–410 (2012).
- [25] R. Adur, C. Du, S. A. Manuilov, H. Wang, F. Yang, D. V. Pelekhov, and P. C. Hammel, The magnetic particle in a box: Analytic and micromagnetic analysis of probe-localized spin wave modes, *J. Appl. Phys.* **117**, 17E108 (2015).
- [26] C. Du, R. Adur, H. Wang, S. A. Manuilov, F. Yang, D. V. Pelekhov, and P. C. Hammel, Experimental and numerical understanding of localized spin wave mode behavior in broadly tunable spatially complex magnetic configurations, *Phys. Rev. B* **90**, 214428 (2014).
- [27] Y. Obukhov, D. V. Pelekhov, J. Kim, P. Banerjee, I. Martin, E. Nazaretski, R. Movshovich, S. An, T. J. Gramila, S. Batra, and P. C. Hammel, Local Ferromagnetic Resonance Imaging with Magnetic Resonance Force Microscopy, *Phys. Rev. Lett.* **100**, 197601 (2008).
- [28] C. Hahn, V. V. Naletov, G. de Loubens, O. Klein, O. d’Allivy Kelly, A. Anane, R. Bernard, E. Jacquet, P. Bortolotti, V. Cros, J. L. Prieto, and M. Munoz, Measurement of the intrinsic damping constant in individual nanodisks of  $Y_3Fe_5O_{12}$  and  $Y_3Fe_5O_{12}/Pt$ , *Appl. Phys. Lett.* **104**, 152410 (2014).
- [29] E. Schlomann, Generation of Spin Waves in Nonuniform Magnetic Fields. I. Conversion of Electromagnetic Power into Spin-Wave Power and Vice Versa, *J. Appl. Phys.* **35**, 159 (1964).
- [30] T. Nan, S. Emori, C. T. Boone, X. Wang, T. M. Oxholm, J. G. Jones, B. M. Howe, G. J. Brown, and N. X. Sun, Comparison of spin-orbit torques and spin pumping across NiFe/Pt and NiFe/Cu/Pt interfaces, *Phys. Rev. B* **91**, 214416 (2015).
- [31] A. Slavin and V. Tiberkevich, Nonlinear Auto-Oscillator Theory of Microwave Generation by Spin-Polarized Current, *IEEE Trans. Magn.* **45**, 1875–1918 (2009).
- [32] See Supplemental Material at [URL will be inserted by publisher] for details of the micromagnetic modeling, the derivation of the resistance shunting factor and estimation of the signal from localized modes, and the current dependence of the resistance.
- [33] Z. Feng, J. Hu, L. Sun, B. You, D. Wu, J. Du, W. Zhang, A. Hu, Y. Yang, D. M. Tang, B. S. Zhang, and H. F. Ding, Spin Hall angle quantification from spin pumping and microwave photoresistance, *Phys. Rev. B* **85**, 214423 (2012).